Ligand-Driven Coordination Sphere-Induced Engineering of Hybride Materials Constructed from PbCl2 and Bis-Pyridyl Organic Linkers for Single-Component Light-Emitting Phosphors

Ligand-driven Engineering of Hybride Materials Constructed from $PbCl_2$ and Bis-pyridyl Organic Linkers: Design of Hitherto Unknown Topologies

Ghodrat Mahmoudi,,[†,‡] Atash V. Gurbanov,[‡,§] Sabina Rodríguez-Hermida,[∥] Rosa Carballo,[∥]*

Mojtaba Amini,[†] Alessia Bacchi,[⊥] Mariusz P. Mitoraj,,[#] Filip Sagan,[#] Mercedes Kukułka,[#] and Damir A. Safin*,[▽]*

[†]Department of Chemistry, Faculty of Science, University of Maragheh, P.O. Box 55181-83111, Maragheh, Iran

[‡]Organic Chemistry Department, RUDN University, Miklukho-Maklaya str. 6, 117198 Moscow, Russian Federation

[§]Department of Chemistry, Baku State University, Z. Xalilov Str. 23, AZ1148, Baku, Azerbaijan

[∥] Departamento de Química Inorgánica, Facultade de Química, Universidade de Vigo, 36310 Vigo, Galicia, Spain

[⊥]Dipartimento di Chimica, Università di Parma, Viale delle Scienze 17A, 43124 Parma, Italy

[#]Department of Theoretical Chemistry, Faculty of Chemistry, Jagiellonian University, R. Ingardena 3, 30-060 Cracow, Poland

▽Institute of Condensed Matter and Nanosciences, Molecules, Solids and Reactivity

(IMCN/MOST), Université catholique de Louvain, Place L. Pasteur 1, 1348 Louvain-la-Neuve,

Belgium

Abstract:

Abstract: We report design and structural characterization of six new coordination polymers fabricated from PbCl2 and a series of closely related bis-pyridyl ligands **LI** and **HLII**–**HLVI**, namely **[Pb2(LI)Cl4]*n***, **[Pb(HLII)Cl2]*n*・nMeOH**, **[Pb(HLIII)Cl2]*n*・0.5nMeOH**, **[Pb2(LIV)Cl3]*n***, **[Pb(HLV)Cl2]*n*** and **[Pb3(LVI)2Cl4]*n*・nMeOH**. The topology of the obtained networks is dictated by the geometry of the organic ligand. The structure of **[Pb2(LI)Cl4]*n*** is constructed from the [PbCl2]*n* 2D sheets, linked through organic linkers into a 3D framework, which exhibits a unique binodal 4,7-connected three-periodic topology named by us as ***sda*1**. Topological analysis of the 2D metal-organic sheet in **[Pb(HLII)Cl2]*n*・nMeOH** discloses a binodal 3,4-connected layer topology, regardless of the presence of tetrel bonds. A 1D coordination polymer **[Pb(HLIII)Cl2]*n*・0.5nMeOH** is considered as a uninodal 2-connected chain. The overall structure of **[Pb2(LIV)Cl3]*n*** is constructed from dimeric tetranuclear [Pb4(μ3-LIV-κ6*N*:*N′*:*N″*:μ3-*O*)2(μ4- Cl)(μ2-Cl)2]3+ cationic blocks linked in a zig-zag manner through bridging μ2-Cl– ligands, yielding a 1D polymeric chain. Topological analysis of this chain reveals a unique pentanodal 3,4,4,5,6-connected chain topology named by us as ***sda*2**. The structure of **[Pb(HLV)Cl2]*n*** exhibits a 1D zig-zag-like polymeric chain. Two chains are further linked into a 1D grid-like ribbon through the dimeric [Pb2(μ2-Cl)2Cl2] blocks as bridging nodes. Using the bulkiest ligand **HLVI**, a 2D layered coordination polymer **[Pb3(LVI)2Cl4]*n*・nMeOH** is formed, which network, considering all tetrel bonds, reveals a unique heptanodal 3,3,3,3,4,5,5-connected layer topology named by us as ***sda*3**. Compounds **[Pb2(LI)Cl4]*n***, **[Pb2(LIV)Cl3]*n*** and **[Pb(HLV)Cl2]*n*** were found to be emissive in the solid state at ambient temperature. While blue emission of **[Pb2(LI)Cl4]*n*** is due to the ligand-centered transitions, bluish green and white luminescence of **[Pb2(LIV)Cl3]*n*** and **[Pb(HLV)Cl2]*n***, respectively, was assigned to LMCT mixed with MC excited states. Molecular as well as periodic calculations have been additionally applied to characterize the obtained polymers.

INTRODUCTION

During the past few decades, rapid progress in the design of photoluminscent coordination compounds for emitting devices has been observed.[1–8] The development of white light-emitting materials is an important target of solid-state lighting research, as these materials, coupled with the appropriate phosphors, offer long lifetime, significant energy savings, and are on track to replace existing mercury containing fluorescent lights. The ability to use a single white lightemitting phosphor clearly would be advantageous. As such, different types of single-component white light-emitting materials, fabricated from coordination compounds, have been developed.[9–15] In this connection, Pb^{II}-based coordination complexes are of interest since Pb^{II}, being a heavy p-block metal ion, possesses a stereochemically active lone pair ($6s^2 6p^0$ electron configuration), which can lead both to interesting structures and luminescence properties.[16–22] The stereochemically active lone pair plays a crucial role in the chemistry of Pb^{II}, which arises from the unique ability of this ion to participate in the formation of tetrel bonds.[23] This supramolecular interaction is formed between a positively charged region on a group 14 atom in continuation of a covalent bond (σ-hole) and an electron donor, analogously to a more common halogen bond. Pb^{II} is particularly prone to the formation of tetrel bonds because of its size and polarizability, as well as its specific hemidirectional coordination,[24] which leaves a gap in the coordination sphere of the Pb^{II} cation (Chart 1), thus enabling the approach of the electron-donor. This makes Pb^{II}-based networks particularly sensitive to the choice of ligands and counter-ions to form supramolecular interactions not only between each other, but also with the metal ion itself.

In this contribution we describe the synthesis, complete structural investigation and topologies of six new Pb^{II} coordination polymers **[Pb$_2$(L^{I})Cl$_4$]$_n$**, **[Pb(HL^{II})Cl$_2$]$_n$ · nMeOH** **[Pb(HL^{III})Cl$_2$]$_n$ · 0.5nMeOH**, **[Pb$_2$(L^{IV})Cl$_3$]$_n$**, **[Pb(HL^{V})Cl$_2$]$_n$** and **[Pb$_3$(L^{VI})$_2$Cl$_4$]$_n$ · nMeOH**, derived from $PbCl_2$ and 1,2-bis(pyridin-3-ylmethylene)hydrazine (**L^{I}**), *N*′-(pyridin-3-ylmethylene)nicotinohydrazide (**HL^{II}**), *N*′-(pyridin-2-ylmethylene)nicotinohydrazide (**HL^{III}**), *N*′-(1-(pyridin-2-yl)ethylidene)picolinohydrazide (**HL^{IV}**), *N*′-(1-(pyridin-2-yl)ethylidene)isonicotinohydrazide (**HL^{V}**) and *N*′-(phenyl(pyridin-2-yl)methylene)nicotinohydrazide (**HL^{VI}**) (Chart 2). The overall topology of the obtained Pb^{II} complexes varies from 1D polymeric chains in **[Pb(HL^{III})Cl$_2$]$_n$ · 0.5nMeOH** and **[Pb$_2$(L^{IV})Cl$_3$]$_n$**, **[Pb(HL^{V})Cl$_2$]$_n$** to 2D metal-organic networks in **[Pb(HL^{II})Cl$_2$]$_n$ · nMeOH**, **[Pb(HL^{V})Cl$_2$]$_n$** and **[Pb$_3$(L^{VI})$_2$Cl$_4$]$_n$ · nMeOH**, and a 3D metal-organic framework in **[Pb$_2$(L^{I})Cl$_4$]$_n$**. We have also demonstrated how an alteration of the orientations of terminal pyridine groups and the bulkiness of the ligand may control the dimensionality and topology of the metal-organic network. Furthermore, the resulting topology of both **[Pb(HL^{V})Cl$_2$]$_n$** and **[Pb$_3$(L^{VI})$_2$Cl$_4$]$_n$ · nMeOH** is highly dictated by the Pb · · · Cl, in the former structure, and Pb · · · Cl and Pb · · · N, in the latter structure, tetrel bonds, highlighting their crucial role for the supramolecular self-assembly of building blocks. Furthermore, it was established that hemidirected coordination of Pb^{II} in the described structures dictates single-component white light-emitting properties. DFT and TDDFT calculations were applied to shed light on the stability of the obtained structures as well as to describe their luminescence properties.

RESULTS AND DISCUSSION

An equimolar one-pot reaction of $PbCl_2$ with a series of closely related organic ligands $\mathbf{L^I}$ or $\mathbf{HL^{II–VI}}$ (Chart 2) in MeOH at 60 °C in a branched tube apparatus leads to heteroleptic complexes $\mathbf{[Pb_2(L^I)Cl_4]_n}$, $\mathbf{[Pb(HL^{II})Cl_2]_n{\cdot}nMeOH}$, $\mathbf{[Pb(HL^{III})Cl_2]_n{\cdot}0.5nMeOH}$, $\mathbf{[Pb_2(L^{IV})Cl_3]_n}$, $\mathbf{[Pb(HL^{V})Cl_2]_n}$ and $\mathbf{[Pb_3(L^{VI})_2Cl_4]_n{\cdot}nMeOH}$, respectively (Scheme 1). Notably, the structures of $\mathbf{[Pb_2(L^{IV})Cl_3]_n}$ and $\mathbf{[Pb_3(L^{VI})_2Cl_4]_n{\cdot}nMeOH}$ each comprise the deprotonated form of the corresponding organic ligand, while the other compounds are constructed from the neutral form of the organic unit.

According to the single crystal X-ray diffraction data, $\mathbf{[Pb_2(L^I)Cl_4]_n}$, $\mathbf{[Pb(HL^{V})Cl_2]_n}$ and $\mathbf{[Pb_3(L^{VI})_2Cl_4]_n{\cdot}nMeOH}$ crystallize in the monoclinic space group $P2_1/c$, while $\mathbf{[Pb_2(L^{IV})Cl_3]_n}$ crystallizes in the monoclinic space group $C2/c$, respectively. Compounds $\mathbf{[Pb(HL^{II})Cl_2]_n{\cdot}nMeOH}$ and $\mathbf{[Pb(HL^{III})Cl_2]_n{\cdot}0.5nMeOH}$ crystallize in the triclinic space group $P\text{–}1$.

The asymmetric unit of $\mathbf{[Pb_2(L^I)Cl_4]_n}$ consists of one Pb^{II} and two Cl^- atoms as well as a half of the ligand $\mathbf{L^I}$. Each Pb^{II} atom is covalently linked to four μ^4-Cl^- and two μ^2-Cl^- atoms, yielding a double layered 2D sheet (Fig. 1, Table 1). These 2D sheets are bridged by the organic linkers, coordinated through the pyridyl nitrogen atoms to the Pb^{II} ions (Table 1), generating a 3D framework (Fig. 1). Thus, each Pb^{II} atom adopts a seven-coordinate coordination geometry. For the sake of topological analysis, the 3D framework of $\mathbf{[Pb_2(L^I)Cl_4]_n}$ was simplified, using the ToposPro software,[47] resulting in a unique binodal 4,7-connected three-periodic topology defined by the point symbol of $(3{\cdot}4^4{\cdot}5)(3^2{\cdot}4^4{\cdot}5^{10}{\cdot}6^5)$ (Fig. 1). Remarkably, this topology was observed for

the first time and named by us as ***sda*1**. The $[PbCl_2]_n$ 2D sheets, in turn, exhibit a binodal 4,6-connected layer topology **4.6L66** defined by the point symbol of $(3{\cdot}4^4{\cdot}6)(3^2{\cdot}4^4{\cdot}5^6{\cdot}6^3)$ (Fig. 1).

The difference between the $\mathbf{HL^{II}}$ and $\mathbf{L^{I}}$ ligands concerns the presence of an amide group in the former compound instead of one of the imine fragments in the latter one (Chart 2). This however leads to quite dramatic changes in the structure of the resulting Pb^{II} CP $\mathbf{[Pb(HL^{II})Cl_2]_n{\cdot}nMeOH}$, the asymmetric unit of which contains one Pb^{II}, two Cl^- atoms, one organic ligand $\mathbf{HL^{II}}$ and one molecule of MeOH. The presence of two 3-pyridyl functions in the structure of $\mathbf{HL^{II}}$ also makes this molecule, similar to $\mathbf{L^{I}}$, incapable of chelating to the Pb^{II} centre, but rather makes $\mathbf{HL^{II}}$ acting as a μ^3-spacer and thus giving rise to the formation of a 2D CP structure (Fig. 2). The six-coordinate Pb^{II} atom is surrounded by two pyridine nitrogen atoms and one carbonyl oxygen atom from three $\mathbf{HL^{II}}$ ligands, as well as three chloride ligands, forming a $[Pb_2(\mu^2\text{-}Cl)_2Cl_2]$ dimer (Fig. 2, Table 1). The bridging chloride ligands are not placed equidistantly between the two lead atoms with the Pb–Cl bonds being 2.716(4) and 3.066(3) Å, while the binding of the terminal chloride ligand shows a 2.696(3) Å distance. The coordination sphere around the metal center in $\mathbf{[Pb(HL^{II})Cl_2]_n{\cdot}nMeOH}$ is hemidirected, which allows the Pb^{II} atom to participate in an additional weak Pb–N tetrel bond of 3.391(11) Å involving the imine nitrogen atom of the O-donating $\mathbf{HL^{II}}$ molecule (Fig. 2). The amide hydrogen atom of the $\mathbf{HL^{II}}$ ligand is involved in the hydrogen bonding with the oxygen atom of the lattice MeOH (Table 2). No other classic hydrogen bonds were found. The 2D CP structure of $\mathbf{[Pb(HL^{II})Cl_2]_n{\cdot}nMeOH}$ is stabilized by efficient π···π stacking interactions (Table 3), formed between the pyridyl rings of the adjacent organic ligands. Topological analysis of the 2D metal-organic sheet in $\mathbf{[Pb(HL^{II})Cl_2]_n{\cdot}nMeOH}$ discloses a binodal 3,4-connected layer topology **3,4L83** defined by the point symbol of

$(4^2 \cdot 6^3 \cdot 8)(4^2 \cdot 6)$ (Fig. 2). It should be noted that tetrel bonds have no influence on the resulting topology.

Replacing the 3-pyridyl group at the imine fragment with a 2-pyridyl one makes the ligand molecule **HL^{III}** (Chart 2) capable of chelating to the Pb^{II} atom with three donor atoms, yielding a 1D CP **[Pb(HL^{III})Cl$_2$]$_n$·0.5nMeOH** (Fig. 3). The asymmetric unit of **[Pb(HL^{III})Cl$_2$]$_n$·0.5nMeOH** consists of one Pb^{II} and two Cl$^-$ atoms as well as one ligand **L^{I}** and a half of the MeOH molecule. The metal atom is also seven-coordinated by two nitrogen and one oxygen atoms from one organic ligand, one 3-pyridyl nitrogen atom from the other organic ligand, two bridging μ^2-Cl$^-$ atoms and one terminal Cl$^-$ atom (Fig. 3, Table 1). The dimeric [Pb$_2$(μ^2-Cl)$_2$Cl$_2$] block is also observed in the structure of **[Pb(HL^{III})Cl$_2$]$_n$·0.5nMeOH**, although its geometry is somewhat different than that observed in **[Pb(HL^{II})Cl$_2$]$_n$·nMeOH**. Particularly, the bridging chloride ligands are almost equidistant from the Pb^{II} centers with the Pb–Cl bonds being 2.884(2) and 2.948(2) Å. The binding of the terminal chloride ligand shows a 2.796(2) Å distance. While the ligand **HL^{III}** chelates one Pb^{II} atom, the 3-pyridyl nitrogen atom of the same ligand binds to a neighboring Pb^{II} center (Fig. 3). Hence, μ^2-**HL^{III}** acts as a linker between the dimeric [Pb$_2$(μ^2-Cl)$_2$Cl$_2$] blocks interconnecting them into 1D chains (Fig. 3). The amide hydrogen atoms of the **HL^{III}** ligands in the structure of **[Pb(HL^{II})Cl$_2$]$_n$·nMeOH** are involved in hydrogen bonding with the terminal Cl$^-$ atoms from the adjacent chains (Table 2), yielding a ladder-like 2D sheet. The hydrogen bonded 2D sheet is further stabilized by π···π stacking interactions (Table 3), formed between the pyridyl rings of the adjacent 1D chains. The metal-organic 1D chain in **[Pb(HL^{III})Cl$_2$]$_n$·0.5nMeOH** can be considered as a uninodal 2-connected chain with the **2C1** topology (Fig. 3).

The difference between the **HL^{IV}** and **HL^{III}** ligands concerns not only the presence of two 2-pyridyl fragments but also the presence of a methyl group on the imine carbon atom (Chart 2). All this leads to dramatic changes in the structure of the resulting Pb^{II} CP **[Pb$_2$(L^{IV})Cl$_3$]$_n$**. The asymmetric unit of this compound consists of one seven- and one six-coordinate Pb^{II} atoms, one ligand **L^{IV}** as well as a half of the bridging μ^4-Cl$^-$ ligand, and two and a half of the bridging μ^2-Cl$^-$ ligands (Table 1). The overall structure of **[Pb$_2$(L^{IV})Cl$_3$]$_n$** is constructed from dimeric tetranuclear [Pb$_4$(μ^3-L^{IV}-κ^6*N*:*N*′:*N*″:μ^3-*O*)$_2$(μ^4-Cl)(μ^2-Cl)$_2$]$^{3+}$ cationic blocks linked in a zig-zag manner through bridging μ^2-Cl$^-$ ligands, yielding a 1D polymeric chain (Fig. 4). The [Pb$_4$(L^{IV})$_2$Cl$_3$]$^{3+}$ building block is symmetric with the 2-fold axis running through the μ^4-Cl$^-$ ligand and orthogonal to the least square plane of the Pb$_2$O$_2$ square-like fragment (Table 1), formed by the two seven-coordinate Pb^{II} atoms and two amide oxygen atoms. The seven-coordinate Pb^{II} atom is in an N$_2$Cl$_3$O$_2$ coordination environment, formed by the two nitrogen and one oxygen atoms from the chelate fragment of one organic ligand **L^{IV}**, one bridging oxygen atom from the other ligand **L^{IV}**, one μ^4-Cl$^-$ ligand and two μ^2-Cl$^-$ ligands. The six-coordinate Pb^{II} atom is in an NCl$_4$O coordination environment, formed by the nitrogen and oxygen atoms of the 2-PyC(O) fragment of the organic ligand, one μ^4-Cl$^-$ ligand and three μ^2-Cl$^-$ ligands. Hence, every μ^3-**L^{IV}**-κ^6*N*:*N*′:*N*″:μ^3-*O* ligand acts as a linker between three Pb^{II} atoms, with the 2-PyC(CH$_3$)N fragment being coordinated to one Pb^{II} atom, the remaining 2-pyridyl nitrogen atom being coordinated to the other Pb^{II} center, and the carbonyl oxygen atom being linked to three metal sites (Fig. 4, Table 1). Topological analysis of the 1D polymeric metal-organic chain in **[Pb$_2$(L^{IV})Cl$_3$]$_n$** discloses a unique pentanodal 3,4,4,5,6-connected chain topology defined by the point symbol of $(3\cdot4^2)_2(3^2\cdot4^2\cdot5^2)(3^2\cdot4^3\cdot5)(3^3\cdot4^3\cdot5^3\cdot6)_2(3^3\cdot4^5\cdot5^5\cdot6^2)_2$ (Fig. 4). Remarkably, this topology was also observed for the first time and named by us as ***sda*2**.

The ligand **HL^{V}**, in comparison with **HL^{IV}**, contains a 4-pyridyl group on the carbonyl side of the molecule. This makes the molecule of **HL^{V}** incapable of chelating to more than one Pb^{II} atoms, but rather makes **HL^{V}** acting as a μ^2-spacer and thus giving rise to the formation of a 1D zig-zag-like polymeric chain **[Pb(HL^{V})Cl$_2$]$_n$** (Fig. 5). The asymmetric unit of **[Pb(HL^{V})Cl$_2$]$_n$** consists of one seven- and one six-coordinate Pb^{II} atoms, two ligands **HL^{V}** as well as one bridging μ^2-Cl$^-$ ligand, and three terminal Cl$^-$ ligands (Table 1). The seven-coordinate Pb^{II} atoms are in the same coordination environment, N_3Cl_3O (Fig. 5), as it was found for the metal atoms in the structure of **[Pb(HL^{III})Cl$_2$]$_n$·0.5nMeOH** (Fig. 3), while the six-coordinate Pb^{II} ions are in an N_3Cl_2O coordination environment. Two 1D zig-zag chains are linked into a 1D grid-like ribbon through the dimeric [Pb$_2$(μ^2-Cl)$_2$Cl$_2$] blocks as bridging nodes, formed by the seven-coordinate Pb^{II} atoms (Fig. 5). These dimeric blocks are quite similar to those in the structure of **[Pb(HL^{III})Cl$_2$]$_n$·0.5nMeOH** with the Pb–μ^2-Cl distances being 2.814(3) and 2.983(4) Å, while the binding of the terminal chloride ligand shows a 2.812(4) Å distance. Interestingly, single-crystal X-ray diffraction studies showed that the six-coordinate Pb^{II} atoms, which serve as terminal nodes of the 1D grid-like ribbon, exhibit a hemidirected coordination geometry, and are involved in tetrel bonding with one of the terminal chloride atoms from the adjacent ribbons (Fig. 5, Table 1). As a result of these interactions, a double-layered 2D sheet is formed. This sheet is further stabilized by $\pi\cdots\pi$ stacking interactions (Table 3), formed between the pyridyl rings of the adjacent ribbons. The topological analysis of **[Pb(HL^{V})Cl$_2$]$_n$**, considering tetrel bonds, revealed a uninodal 3-connected plane topology **hcb** (Shubnikov hexagonal plane net) defined by the point symbol of (6^3), while the same analysis without tetrel bonds yields a **SP 1-periodic net** (4,4)(0,2) topology (Fig. 5).

The ligand **HL^{VI}** is the bulkiest one among the exploited ligands in this work, and its structure resembles that of **HL^{III}**, although containing a phenyl fragment on the imine carbon atom (Chart 2). Despite of the presence of bulky phenyl fragment, a 2D layered CP **[Pb$_3$(L^{VI})$_2$Cl$_4$]$_n$·nMeOH** is formed (Fig. 6). The asymmetric unit of this compound consists of two five- and one four-coordinate Pb^{II} atoms, two organic ligands **L^{VI}** as well as two bridging μ^2-Cl$^-$ ligands, and two terminal Cl$^-$ ligands (Fig. 6, Table 1). Every **L^{VI}** ligand acts, considering only covalent bonds (Table 1), as a μ^2-linker, chelating one Pb^{II} center with three atoms and coordinating the other Pb^{II} center through the 3-pyridyl nitrogen atom. One of the five-coordinate Pb^{II} atoms is in an N_2Cl_2O coordination environment formed by the chelate fragment of **L^{VI}** and two μ^2-Cl$^-$ ligands, while the other five-coordinate Pb^{II} atom is in an N_2Cl_3 coordination environment formed by two nitrogen atoms from two 3-pyridyl fragments of two **L^{VI}** as well as two μ^2-Cl$^-$ ligands and one terminal Cl$^-$ ligand. The four-coordinate Pb^{II} atom is in an N_2ClO coordination environment thanks to the chelating fragment of **L^{VI}** and one terminal Cl$^-$ ligand. Notably, each Pb^{II} atom exhibits a hemidirected coordination geometry, and are involved in tetrel bonding with one of the terminal chloride atoms from the adjacent ribbons (Fig. 5, Table 1). Particularly, the N_2Cl_2O coordinated Pb^{II} atom forms a tetrel bond with the amide nitrogen atom from the adjacent ligand **L^{VI}**, while the N_2Cl_3 coordinated Pb^{II} ion is involved in tetrel bonding with the adjacent terminal Cl$^-$ ligand, arising from the covalent coordination sphere of the four-coordinate metal atom (Fig. 6, Table 1). The latter metal center, in turn, forms three tetrel bonds: one bond with the amide nitrogen atom from the adjacent ligand **L^{VI}** and two bonds with the bridging μ^2-Cl$^-$ ligands (Fig. 6, Table 1). The 2D layered structure of **[Pb$_3$(L^{VI})$_2$Cl$_4$]$_n$·nMeOH** is stabilized by π···π stacking interactions (Table 3), formed between the pyridyl rings of the adjacent organic ligands. Furtermore, one of the terminal Cl$^-$ ligands is involved in intermolecular hydrogen bonding with the OH hydrogen atom of the lattice MeOH molecule (Table 2). A simplified underlying network

of **[Pb$_3$(L^{VI})$_2$Cl$_4$]$_n$·nMeOH**, considering all tetrel bonds, reveals a unique heptanodal 3,3,3,3,4,5,5-connected layer topology defined by the point symbol of $(3{\cdot}4{\cdot}5)(3{\cdot}4^2{\cdot}6{\cdot}7^2{\cdot}8^2{\cdot}9^2)(3{\cdot}4^3{\cdot}5{\cdot}6^2{\cdot}7^2{\cdot}8)(4^2{\cdot}6)_2(4^3{\cdot}6^2{\cdot}7)(4^3)$ (Fig. 6). This topology was also observed for the first time and named by us as ***sda*3**. The topological analysis of **[Pb$_3$(L^{VI})$_2$Cl$_4$]$_n$·nMeOH**, considering only Pb···N tetrel bonds, reveals a unique tetranodal 3,3,4,4-connected layer topology **3,3,4,4L1** defined by the point symbol of $(3{\cdot}8^2)(3{\cdot}8^4{\cdot}9)(3^2{\cdot}4{\cdot}8^2{\cdot}9)(3^2{\cdot}4)$ (Fig. 7). The same analysis, considering only Pb···Cl tetrel bonds, yields also a unique pentanodal 3,3,3,4,5-connected layer topology **3,3,3,4,5L1** defined by the point symbol of $(3{\cdot}4{\cdot}5^2{\cdot}6^2)(3{\cdot}4{\cdot}5)(3{\cdot}5^2{\cdot}6^4{\cdot}8{\cdot}9^2)(4{\cdot}5{\cdot}6)(4{\cdot}6^2)$ (Fig. 7). However, if all the tetrel bonds are excluded from the topological analysis, a simplified underlying network of **[Pb$_3$(L^{VI})$_2$Cl$_4$]$_n$·nMeOH** exhibits a uninodal 3-connected plane topology **hcb** (Shubnikov hexagonal plane net) defined by the point symbol of (6^3) (Fig. 7).

EXPERIMENTAL SECTION

Materials. All ligands were prepared following the reported method as described elsewhere.[48] All other reagents and solvents were commercially available and used as without further purification.

Physical measurements. Microanalyses were performed using a Heraeus CHN-O-Rapid analyzer. Melting points were measured on an Electrothermal 9100 apparatus.

Synthesis of complexes. $PbCl_2$ (0.139 g, 0.5 mmol) and the corresponding ligand **L^{I}** or **HL^{II}–HL^{VI}** (0.105, 0.113, 0.113, 0.120, 0.120 and 0.151 g, rerspectively; 0.5 mmol) were placed in the main arm of a branched tube. MeOH (15 mL) was carefully added to fill the arms. The tube was

sealed and immersed in an oil bath at 60 °C while the branched arm was kept at ambient temperature. X-ray suitable crystals were formed during the next days in the cooler arm and were filtered off, washed with acetone and diethyl ether, and dried in air.

$[Pb_2(L^{I})Cl_4]_n$. Yellow plate-like crystals. Yield: 0.155 g (81%). M. p. 190 °C, *Anal*. Calc. for $C_{12}H_{10}Cl_4N_4Pb_2$ (766.45) (%): C 18.81, H 1.32 and N 7.31; found: C 18.70, H 1.23 and N 7.25.

$[Pb(HL^{II})Cl_2]_n$·nMeOH. Yellow prism-like crystals. Yield: 0.228 g (85%). M. p. 201 °C, *Anal*. Calc. for $C_{13}H_{14}Cl_2N_4O_2Pb$ (536.39) (%): C 29.11, H 2.63 and N 10.45; found C 28.91, H 2.71 and N 11.00

$[Pb(HL^{III})Cl_2]_n$·0.5nMeOH. Yellow block-like crystals. Yield: 0.174 g (67%). M. p. 255 °C, *Anal*. Calc. for $C_{12.5}H_{12}Cl_2N_4O_{1.5}Pb$ (520.37) (%): C 28.85, H 2.32 and N 10.77; found C 29.01, H 2.50 and N 11.07 .

$[Pb_2(L^{IV})Cl_3]_n$. Yellow block-like crystals. Yield: 0.124 g (65%). M. p. 294 °C, *Anal*. Calc. for $C_{13}H_{11}Cl_3N_4OPb_2$ (760.02) (%): C 20.54, H 1.46 and N 7.37; found: C 20.15, H 1.51 and N 7.57.

$[Pb(HL^{V})Cl_2]_n$. Green parallelepiped-like crystals. Yield: 0.233 g (90%). M. p. 287 °C, *Anal*. Calc. for $C_{13}H_{12}Cl_2N_4OPb$ (518.37) (%): C 30.12, H 2.33 and N 10.81; found: C 30.24, H 2.17 and N 10.97 **.**

$[Pb_3(L^{VI})_2Cl_4]_n$·nMeOH. Yellow needle-like crystals. Yield: 0.168 g (72%). M. p. 239 °C, *Anal*. Calc. for $C_{37}H_{30}Cl_4N_8O_3Pb_3$, (1398.11) (%): C 31.79, H 2.16 and N 8.01; found: C 31.99, H 2.02 and N 8.17.

Single-crystal X-ray diffraction. The X-ray data were collected on a Bruker four-circle single crystal diffractometers with a sealed graphite-monochromatised Mo-Kα (λ = 0.71073 Å) radiation tube and an APEX-II CCD detector. The frames were integrated with the Bruker SAINT software package,[49] and the data were corrected for absorption using the program SADABS.[50] The structures were solved by direct methods using the program SHELXS97.[51] Non-hydrogen atoms were refined with the full-matrix least-squares procedure on $|F^2|$ by SHELXL97.[51] Hydrogen atoms were inserted at calculated positions and constrained with isotropic thermal parameters. Figures were generated using the program Mercury.[52]

Crystal data for $[Pb_2(L^I)Cl_4]_n$. $C_{12}H_{10}Cl_4N_4Pb_2$, M_r = 766.42 g mol^{-1}, T = 173(2) K, monoclinic, space group $P2_1/c$, a = 17.527(4), b = 7.2591(15), c = 7.4711(15) Å, β = 93.66(3)°, V = 948.6(4) Å^3, Z = 2, ρ = 2.683 g cm^{-3}, μ(Mo-Kα) = 18.287 mm^{-1}, reflections: 4907 collected, 1705 unique, R_{int} = 0.070, R_1(all) = 0.0710, wR_2(all) = 0.1212.

Crystal data for $[Pb(HL^{II})Cl_2]_n$·nMeOH. $C_{12}H_{10}Cl_2N_4OPb$, CH_4O; M_r = 536.37 g mol^{-1}, T = 173(2) K, triclinic, space group P–1, a = 8.5656(5), b = 9.1844(5), c = 11.0989(8) Å, α = 95.431(5), β = 109.809(6), γ = 90.393(6)°, V = 817.09(9) Å^3, Z = 2, ρ = 2.164 g cm^{-3}, μ(Mo-Kα) = 10.662 mm^{-1}, reflections: 6366 collected, 3762 unique, R_{int} = 0.064, R_1(all) = 0.0902, wR_2(all) = 0.1579.

Crystal data for $[Pb(HL^{III})Cl_2]_n$·0.5nMeOH. $C_{12}H_{10}Cl_2N_4OPb$, 0.5(CH_4O); M_r = 520.33 g mol^{-1}, T = 293(2) K, triclinic, space group P–1, a = 8.5656(5), b = 10.6025(12), c = 10.6335(12) Å, α = 95.295(2), β = 103.359(2), γ = 99.606(2)°, V = 788.95(15) Å^3, Z = 2, ρ = 2.191 g cm^{-3}, μ(Mo-Kα) = 11.030 mm^{-1}, reflections: 12624 collected, 4718 unique, R_{int} = 0.068, R_1(all) = 0.0592, wR_2(all) = 0.1077.

Crystal data for $[Pb_2(L^{IV})Cl_3]_n$. $C_{13}H_{11}Cl_3N_4OPb_2$, M_r = 759.99 g mol^{-1}, T = 110(2) K, monoclinic, space group $C2/c$, a = 24.8751(9), b = 9.7305(3), c = 15.5416(5) Å, β = 113.718(2)°, V = 3444.1(2) Å^3, Z = 8, ρ = 2.931 g cm^{-3}, μ(Mo-Kα) = 20.000 mm^{-1}, reflections: 24128 collected, 6242 unique, R_{int} = 0.032, R_1(all) = 0.0338, wR_2(all) = 0.0520.

Crystal data for $[Pb(HL^{V})Cl_2]_n$. $C_{13}H_{12}Cl_2N_4OPb$, M_r = 518.36 g mol^{-1}, T = 293(2) K, monoclinic, space group $P2_1/c$, a = 14.5358(5), b = 15.6284(3), c = 13.7627(5) Å, β = 105.206(3)°, V = 3017.03(17) Å^3, Z = 8, ρ = 2.282 g cm^{-3}, μ(Mo-Kα) = 11.541 mm^{-1}, reflections: 13688 collected, 5513 unique, R_{int} = 0.070, R_1(all) = 0.0715, wR_2(all) = 0.1305.

Crystal data for $[Pb_3(L^{VI})_2Cl_4]_n$·nMeOH. $C_{36}H_{26}Cl_4N_8O_2Pb_3$, CH_4O; M_r = 1398.06 g mol^{-1}, T = 293(2) K, monoclinic, space group $P2_1/c$, a = 21.544(5), b = 9.544(2), c = 19.074(4) Å, β = 100.415(4)°, V = 3857.3(15) Å^3, Z = 4, ρ = 2.408 g cm^{-3}, μ(Mo-Kα) = 13.388 mm^{-1}, reflections: 20013 collected, 6814 unique, R_{int} = 0.123, R_1(all) = 0.1466, wR_2(all) = 0.1664.

CCDC 1497457–1497462 contain the supplementary crystallographic data. This data can be obtained free of charge via http://www.ccdc.cam.ac.uk/conts/retrieving.html, or from the Cambridge Crystallographic Data Centre, 12 Union Road, Cambridge CB2 1EZ, UK; fax: (+44) 1223-336-033; or e-mail: deposit@ccdc.cam.ac.uk.

CONCLUSIONS

In summary, we have designed and fully structurally characterized six new coordination polymers, namely **$[Pb_2(L^{I})Cl_4]_n$**, **$[Pb(HL^{II})Cl_2]_n$·nMeOH**, **$[Pb(HL^{III})Cl_2]_n$·0.5nMeOH**, **$[Pb_2(L^{IV})Cl_3]_n$**, **$[Pb(HL^{V})Cl_2]_n$** and **$[Pb_3(L^{VI})_2Cl_4]_n$·nMeOH**, fabricated from $PbCl_2$ and a series

of closely related bis-pyridyl ligands $\mathbf{L^{I}}$ and $\mathbf{HL^{II}}$–$\mathbf{HL^{VI}}$. Based on the structural analysis, we conclude that the topology of the obtained networks is dictated by the geometry of the organic ligand.

The structure of $\mathbf{[Pb_2(L^{I})Cl_4]_{\mathit{n}}}$ is constructed from the $[PbCl_2]_n$ 2D sheets, linked through organic linkers into a 3D framework, which exhibits a unique binodal 4,7-connected three-periodic topology named by us as ***sda*1**. The $[PbCl_2]_n$ 2D sheets, in turn, exhibit a binodal 4,6-connected layer topology **4.6L66**. The coordination sphere around the metal center in the 2D coordination polymer $\mathbf{[Pb(HL^{II})Cl_2]_{\mathit{n}}\cdot nMeOH}$ is hemidirected, which allows the Pb^{II} atom to participate in an additional weak Pb–N tetrel bond. Topological analysis of the 2D metal-organic sheet in $\mathbf{[Pb(HL^{II})Cl_2]_{\mathit{n}}\cdot nMeOH}$ discloses a binodal 3,4-connected layer topology **3,4L83**, regardless of tetrel bonds. A 1D coordination polymer $\mathbf{[Pb(HL^{III})Cl_2]_{\mathit{n}}\cdot 0.5nMeOH}$ is considered as a uninodal 2-connected chain with the **2C1** topology. The overall structure of $\mathbf{[Pb_2(L^{IV})Cl_3]_{\mathit{n}}}$ is constructed from dimeric tetranuclear $[Pb_4(\mu^3\text{-}L^{IV}\text{-}\kappa^6\mathit{N}\mathit{:}\mathit{N'}\mathit{:}\mathit{N''}\mathit{:}\mu^3\text{-}\mathit{O})_2(\mu^4\text{-}Cl)(\mu^2\text{-}Cl)_2]^{3+}$ cationic blocks linked in a zig-zag manner through bridging μ^2-Cl^- ligands, yielding a 1D polymeric chain. Topological analysis of this chain reveals a unique pentanodal 3,4,4,5,6-connected chain topology named by us as ***sda*2**. The structure of $\mathbf{[Pb(HL^{V})Cl_2]_{\mathit{n}}}$ exhibits a 1D zig-zag-like polymeric chain. Two chains are further linked into a 1D grid-like ribbon through the dimeric $[Pb_2(\mu^2\text{-}Cl)_2Cl_2]$ blocks as bridging nodes. Single-crystal X-ray diffraction studies showed that the Pb^{II}-based terminal nodes of the 1D grid-like ribbon exhibit a hemidirected coordination geometry, and are involved in tetrel bonding with one of the terminal chloride atoms from the adjacent ribbons. As a result of these interactions, a double-layered 2D sheet is formed. The topological analysis of $\mathbf{[Pb(HL^{V})Cl_2]_{\mathit{n}}}$, considering tetrel bonds, revealed a uninodal 3-connected plane topology **hcb** (Shubnikov hexagonal plane net), while the same analysis without tetrel bonds yields a **SP 1-**

periodic net (4,4)(0,2) topology. Using the bulkiest, among the exploited in this work, ligand **HL^{VI}** a 2D layered coordination polymer **[Pb$_3$(L^{VI})$_2$Cl$_4$]$_n$·nMeOH** is formed, which network, considering all tetrel bonds, reveals a unique heptanodal 3,3,3,3,4,5,5-connected layer topology named by us as ***sda*3**. The topological analysis of **[Pb$_3$(L^{VI})$_2$Cl$_4$]$_n$·nMeOH**, considering only Pb···N tetrel bonds, reveals a unique tetranodal 3,3,4,4-connected layer topology **3,3,4,4L1**, while the same analysis, considering only Pb···Cl tetrel bonds, yields also a unique pentanodal 3,3,3,4,5-connected layer topology **3,3,3,4,5L1**. If all the tetrel bonds are excluded from the topological analysis, a simplified underlying network of **[Pb$_3$(L^{VI})$_2$Cl$_4$]$_n$·nMeOH** exhibits a uninodal 3-connected plane topology **hcb** (Shubnikov hexagonal plane net).

Thus, tetrel bonding can play a key role for the supramolecular aggregation of building units in solid state and can legally be considered as one of the most powerful tool to design metal-organic frameworks with different dimensionalities and topologies, as evidenced from the reported in this work hitherto unknown topologies ***sda*1**, ***sda*2** and ***sda*3**.

AUTHOR INFORMATION

Corresponding Authors

*E-mail: mahmoudi_ghodrat@yahoo.co.uk (G. Mahmoudi).

*E-mail: damir.a.safin@gmail.com (D. A. Safin).

Notes

The authors declare no competing financial interest.

ACKNOWLEDGEMENTS

This work was supported by the Ministry of Education and Science of the Russian Federation (the Agreement number 02.a03.21.0008)

REFERENCES

(1) *Alfred Werner – Biographical*, Nobelprize.org., Nobel Media AB, **2013**. Web. 26 Jan 2014; http://www.nobelprize.org/nobel_prizes/chemistry/laureates/1913/werner-bio.html.

(2) Constable, E. C.; Housecroft, C. E. *Chem. Soc. Rev.* **2013**, *42*, 1429.

(3) Werner, H. *Angew. Chem., Int. Ed.* **2013**, *52*, 6146.

(4) Stadler, A.-M.; Harrowfield, J.; Ramírez, J. *Polyhedron* **2013**, *52*, 1465.

(5) Zhang, J. P.; Huang, X. C.; Chen, X. M. *Chem. Soc. Rev.* **2009**, *38*, 2385.

(6) Farha, O. K.; Hupp, J. T. *Acc. Chem. Res.* **2010**, *43*, 1166.

(7) Kitagawa, S.; Matsuda, R. *Coord. Chem. Rev.* **2007**, *251*, 2490.

(8) Cohen, S. M.; Wang, Z. Q. *Chem. Soc. Rev.* **2009**, *38*, 1315.

(9) Ma, Z. B.; Moulton, B. *Coord. Chem. Rev.* **2011**, *255*, 1623.

(10) Coronado, E.; Mínguez Espallargas, G. *Chem. Soc. Rev.* **2013**, *42*, 1525.

(11) Fabbrizzi, L.; Poggi, A. *Chem. Soc. Rev.* **2013**, *42*, 1681.

(12) Frischmann, P. D.; Mahata, K.; Würthner, F. *Chem. Soc. Rev.* **2013**, *42*, 1847.

(13) Stock, N.; Biswas, S. *Chem. Rev.* **2012**, *112*, 933.

(14) Yaghi, O. M.; Li, H.; Groy, T. L. *Inorg. Chem.* **1997**, *36*, 4292.

(15) Wagner, B. D.; McManus, G. J.; Moulton, B.; Zaworotko, M. J. *Chem. Commun.* **2002**, 2176.

(16) Beatty, A. M. *Coord. Chem. Rev.* **2003**, *246*, 131.

(17) Chen, C.-L.; Kang, B.-S.; Su, C.-Y. *Aust. J. Chem.* **2006**, *59*, 3.

(18) Li, X.-P.; Zhang, J.-Y.; Pan, M.; Zheng, S.-R.; Liu, Y.; Su, C.-Y. *Inorg. Chem.* **2007**, *46*, 4617.

(19) Ruben, M.; Rojo, J.; Romero-Salguero, F. J.; Uppadine, L. H.; Lehn, J.-M. *Angew. Chem., Int. Ed.* **2004**, *43*, 3644.

(20) Ruben, M.; Lehn, J.-M.; Müller, P. *Chem. Soc. Rev.* **2006**, *35*, 1056.

(21) Milway, V. A.; Abedin, S. M. T.; Niel, V.; Kelly, T. L.; Dawe, L. N.; Dey, S. K.; Thompson, D. W.; Miller, D. O.; Alam, M. S.; Müller, P.; Thompson, L. K. *Dalton Trans.* **2006**, 2835.

(22) Dawe, L. N.; Abedin, T. S. M.; Thompson, L. K. *Dalton Trans.* **2008**, 1661.

(23) Dawe, L. N.; Shuvaev, K. V.; Thompson, L. K. *Chem. Soc. Rev.* **2009**, *38*, 2334.

(24) Dawe, L. N.; Shuvaev, K. V.; Thompson, L. K. *Dalton Trans.* **2009**, 3323.

(25) Du, Z. Y.; Xu, H. B.; Li, X. L.; Mao, J. G. *Eur. J. Inorg. Chem.* **2007**, 4520.

(26) Thirumurugan, A.; Sanguramath, R. A.; Rao, C. N. R. *Inorg. Chem.* **2008**, *47*, 823.

(27) Yang, J.; Ma, J. F.; Liu, Y. Y.; Ma, J. C.; Batten, S. R. *Cryst. Growth Des.* **2009**, *9*, 1894.

(28) Ding, B.; Liu, Y. Y.; Wu, X. X.; Zhao, X. J.; Du, G. X.; Yang, E. C.; Wang, X. G. *Cryst. Growth Des.* **2009**, *9*, 4176.

(29) Li, S. H.; Gao, S. K.; Liu, S. X.; Guo, Y. N. *Cryst. Growth Des.* **2010**, *10*, 495.

(30) Li, D. S.; Wu, Y. P.; Zhang, P.; Du, M.; Zhao, J.; Li, C. P.; Wang, Y. Y. *Cryst. Growth Des.* **2010**, *10*, 2037.

(31) Wang, X. L.; Chen, Y. Q.; Gao, Q.; Lin, H. Y.; Liu, G. C.; Zhang, J. X.; Tian, A. X. *Cryst. Growth Des.* **2010**, *10*, 2174.

(32) Yang, G. P.; Hou, L.; Wang, Y. Y.; Zhang, Y. N.; Shi, Q. Z.; Batten, S. R. *Cryst. Growth Des.* **2011**, *11*, 936.

(33) Liu, T. F.; Lu, J.; Tian, C. B.; Cao, M. N.; Lin, Z. J.; Cao, R. *Inorg. Chem.* **2011**, *50*, 2264.

(34) Bauzá, A.; Mooibroek, T. J.; Frontera, A. *Chem. Rec.* **2016**, *16*, 473.

(35) Davidovich, R. L.; Stavila, V.; Marinin, D. V.; Voit, E. I.; Whitmire, K. H. *Coord. Chem. Rev.* **2009**, *253*, 1316.

(36) Safin, D. A.; Frost, J.; Murugesu, M. *Dalton Trans.* **2015**, *44*, 20287.

(37) Case, F. H.; Koft, E. *J. Am. Chem. Soc.* **1959**, *81*, 905.

(38) Lerner, E. I.; Lippard, S. J. *Inorg. Chem.* **1977**, *16*, 1537.

(39) Garcia, A. M.; Bassani, D. M.; Lehn, J.-M.; Baum, G.; Fenske, D. *Chem. Eur. J.* **1999**, *5*, 1234.

(40) Safin, D. A.; Xu, Y.; Korobkov, I.; Bryce, D. L.; Murugesu, M. *CrystEngComm* **2013**, *15*, 10419.

(41) Safin, D. A.; Tumanov, N. A.; Leitch, A. A.; Brusso, J. L.; Filinchuk, Y.; Murugesu, M. *CrystEngComm* **2015**, *17*, 2190.

(42) Safin, D. A.; Burgess, K. M. N.; Korobkov, I.; Bryce, D. L.; Murugesu, M. *CrystEngComm* **2014**, *14*, 3466.

(43) Safin, D. A.; Holmberg, R. J.; Burgess, K. M. N.; Robeyns, K.; Bryce, D. L.; Murugesu, M. *Eur. J. Inorg. Chem.* **2015**, 441.

(44) Safin, D. A.; Pialat, A.; Korobkov, I.; Murugesu, M. *Chem. Eur. J.* **2015**, *21*, 6144.

(45) Safin, D. A.; Pialat, A.; Leitch, A. A.; Tumanov, N. A.; Korobkov, I.; Filinchuk, Y.; Brusso, J. L.; Murugesu, M. *Chem Commun.* **2015**, *51*, 9547.

(46) Safin, D. A.; Szell, P. M. J.; Keller, A.; Korobkov, I.; Bryce, D. L.; Murugesu, M. *New J. Chem.* **2015**, *39*, 7147.

(47) Blatov, V. A.; Shevchenko, A. P.; Proserpio, D. M. *Cryst. Growth Des.* **2014**, *14*, 3576.

(48) Case, F. H. *J. Heterocycl. Chem.* **1973**, *10*, 353.

(49) Siemens SAINT, Version 4, Software Reference Manual, Siemens Analytical X-Ray Systems, Inc., Madison, WI, USA, **1996**.

(50) Sheldrick, G. M. SADABS, Program for Empirical Absorption Correction of Area Detector Data, University of Göttingen, Germany, **1996**.

(51) Sheldrick, G. M. Program for the Solution of Crystal Structures from X-Ray Data, University of Göttingen, Germany, **1997**.

(52) Macrae, C. F., Bruno, I. J., Chisholm, J. A., Edgington, P. R., McCabe, P., Pidcock, E., Rodriguez-Monge, L., Taylor, R., van de Streek, J.; Wood, P. A. *J. Appl. Cryst.* **2008**, *41*, 466.

For Table of Contents Use Only

Ligand-driven Engineering of Hybride Materials Constructed from PbCl2 and Bis-pyridyl Organic Linkers: Design of Hitherto Unknown Topologies

Ghodrat Mahmoudi,,[†,‡] Atash V. Gurbanov,[‡,§] Sabina Rodríguez-Hermida,[∥] Rosa Carballo,[∥] Mojtaba Amini,[†] Alessia Bacchi,[⊥] Mariusz P. Mitoraj,*,[#] Filip Sagan,[#] Mercedes Kukułka,[#] and Damir A. Safin*,[▽]*

Six new Pb^{II} coordination polymers were assembled from $PbCl_2$ and a series of closely related ligands $\mathbf{L^I}$ and $\mathbf{HL^{II}}$–$\mathbf{HL^{VI}}$. Their detailed structural and topological analyses are discussed. It was established, that tetrel bonding, found in some of the obtained compounds can play a key role for the supramolecular aggregation of building units in solid state and is legally considered as one of the most powerful tool to design metal-organic frameworks with different dimensionalities and topologies.

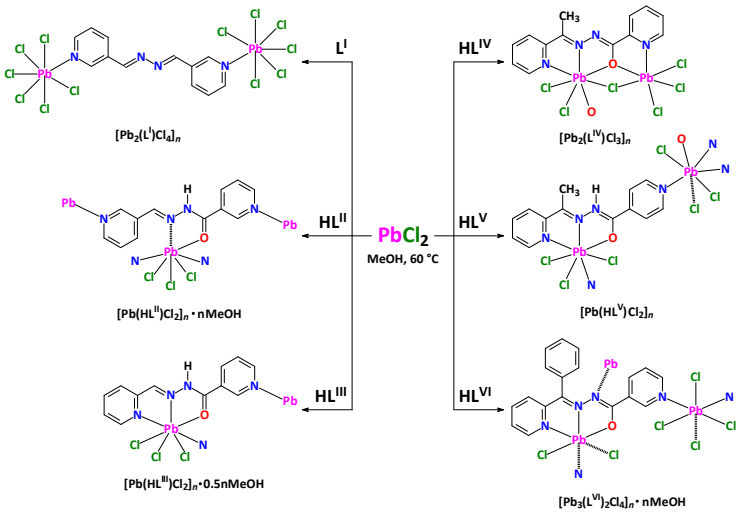

Chart 1. The simplified diagram of the holodirected and hemidirected coordination spheres around lead

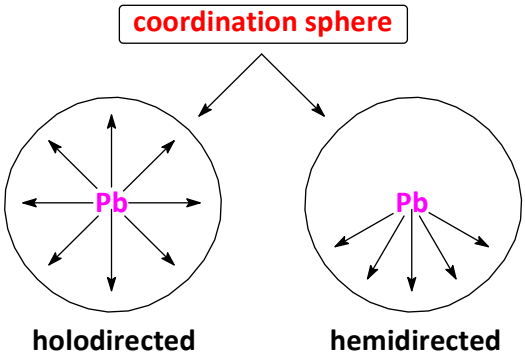

Chart 2. Diagrams of the employed ligands L^{I} and HL^{II}–HL^{VI}

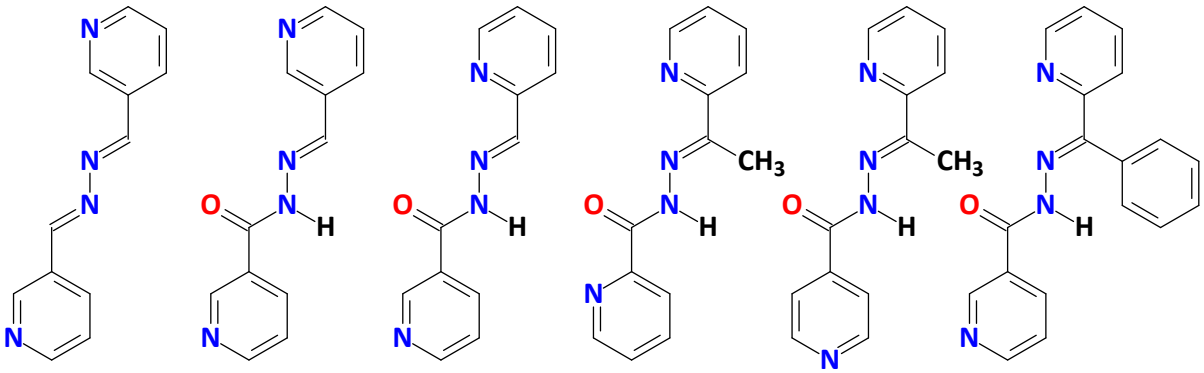

Scheme 1. Syntheses of Pb^{II} complexes described in this work. Tetrel bonds are shown as dashed lines.

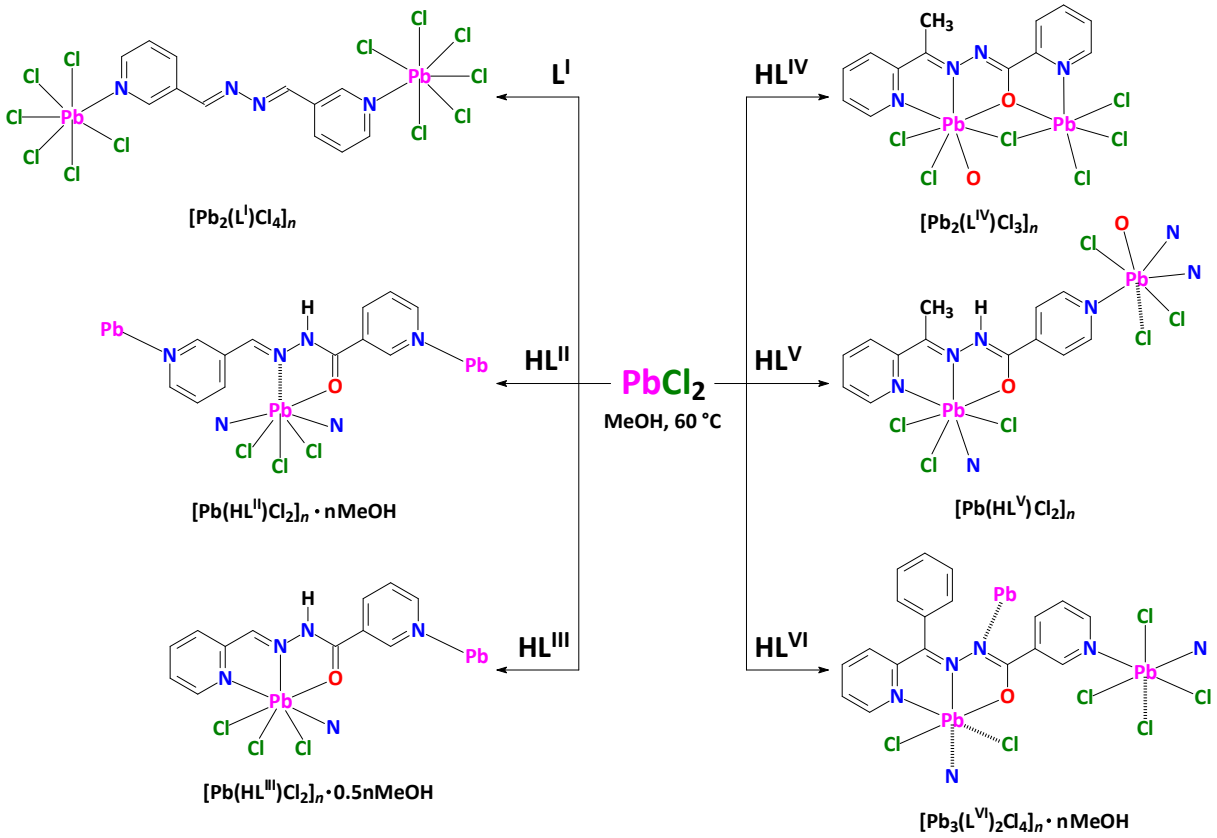

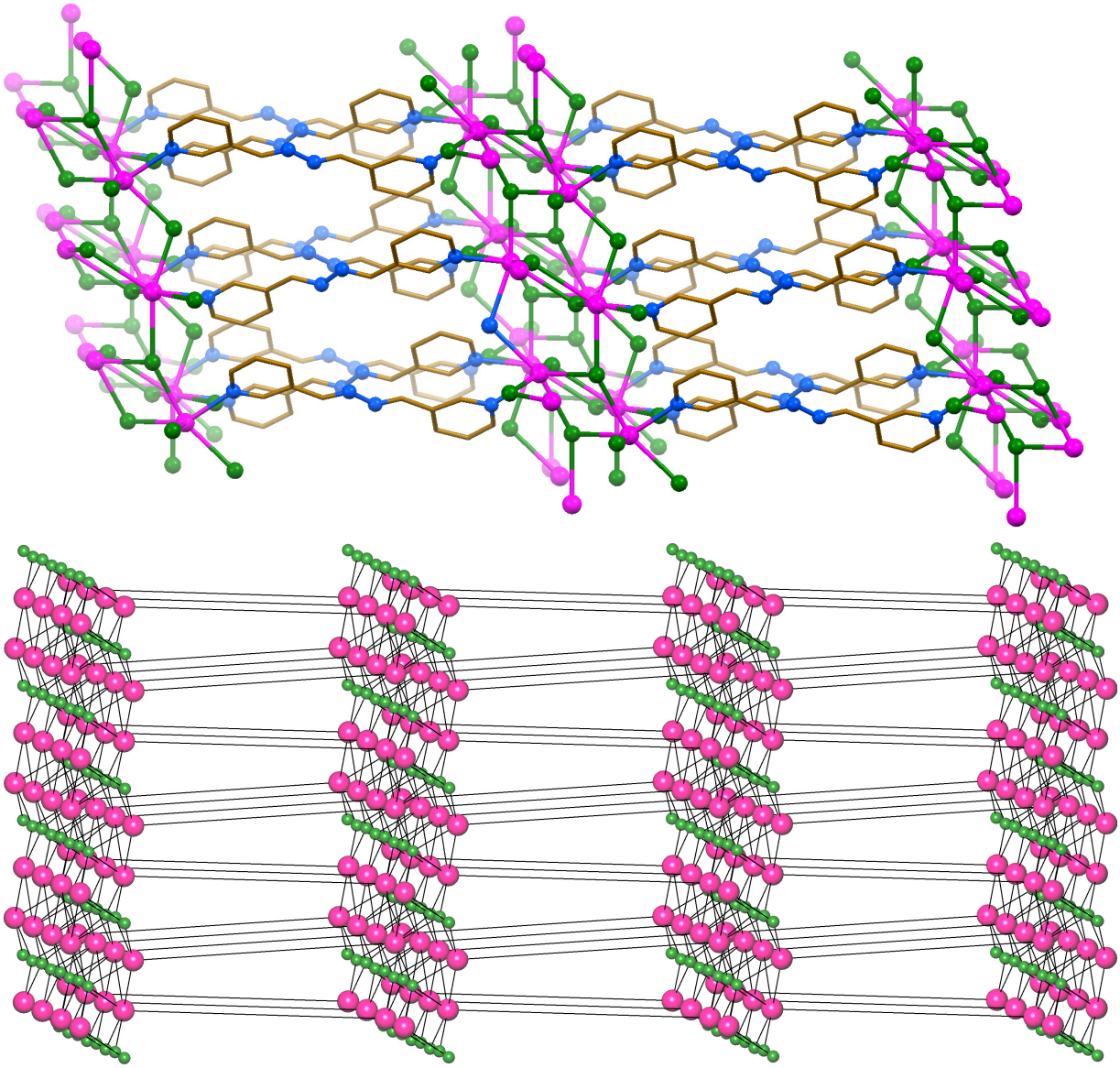

Figure 1. (top) Crystal structure of **[$Pb_2(L^I)Cl_4$]$_n$** (hydrogen atoms are omitted for clarity; color code: C = gold, N = blue, Cl = green, Pb = magenta). (bottom) A simplified underlying network of **[$Pb_2(L^I)Cl_4$]$_n$** with the unique binodal 4,7-connected three-periodic topology ***sda*1** defined by the point symbol of $(3\cdot4^4\cdot5)(3^2\cdot4^4\cdot5^{10}\cdot6^5)$, and constructed from layers with the binodal 4,6-connected layer topology **4.6L66** defined by the point symbol of $(3\cdot4^4\cdot6)(3^2\cdot4^4\cdot5^6\cdot6^3)$ (color code: Cl = green, Pb = magenta).

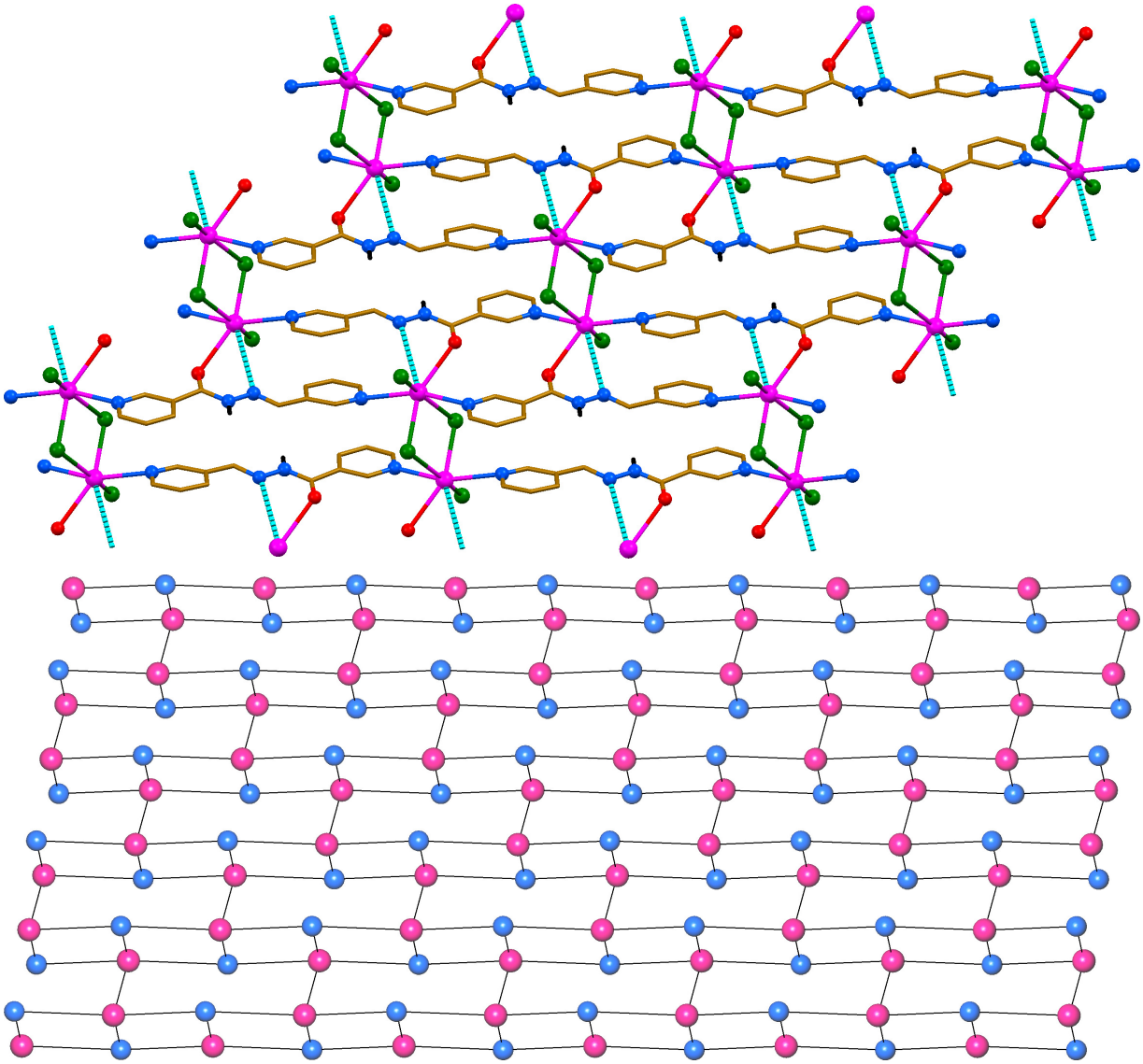

Figure 2. (top) Crystal structure of **[Pb(HL^{II})Cl$_2$]$_n$·nMeOH** (CH hydrogen atoms and methanol molecules are omitted for clarity; color code: C = gold, N = blue, Cl = green, O = red, Pb = magenta). Tetrel bonds Pb···N are shown as dashed lines. (bottom) A simplified underlying network of **[Pb(HL^{II})Cl$_2$]$_n$·nMeOH**, considering and without tetrel bonds, with the binodal 3,4-connected layer topology **3,4L83** defined by the point symbol of $(4^2{\cdot}6^3{\cdot}8)(4^2{\cdot}6)$ (color code: **HL^{II}** = blue, Pb = magenta).

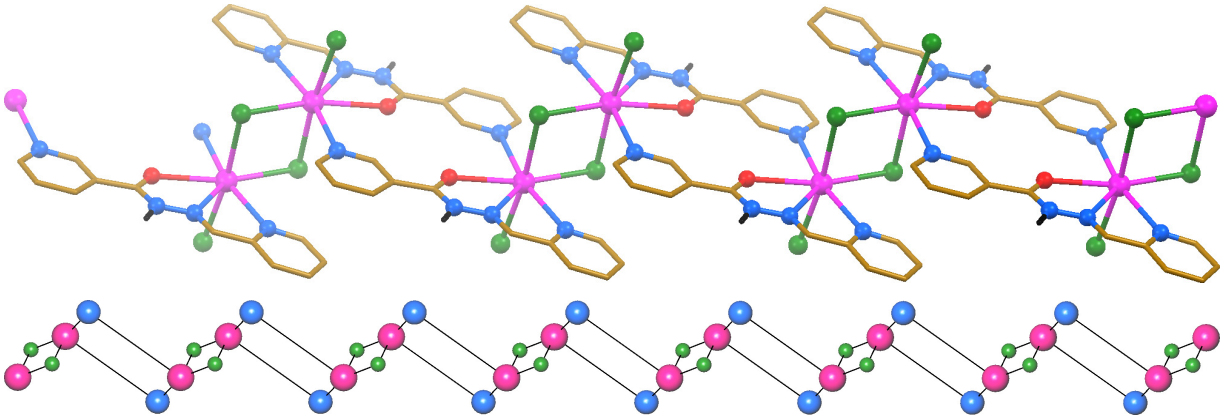

Figure 3. (top) Crystal structure of **[Pb(HL^{III})Cl$_2$]$_n$·0.5nMeOH** (CH hydrogen atoms and methanol molecules are omitted for clarity; color code: C = gold, N = blue, Cl = green, O = red, Pb = magenta). (bottom) A simplified underlying network of **[Pb(HL^{III})Cl$_2$]$_n$·0.5nMeOH** with the uninodal 2-connected chain topology **2C1** (color code: **HL^{III}** = blue, Cl = green, Pb = magenta).

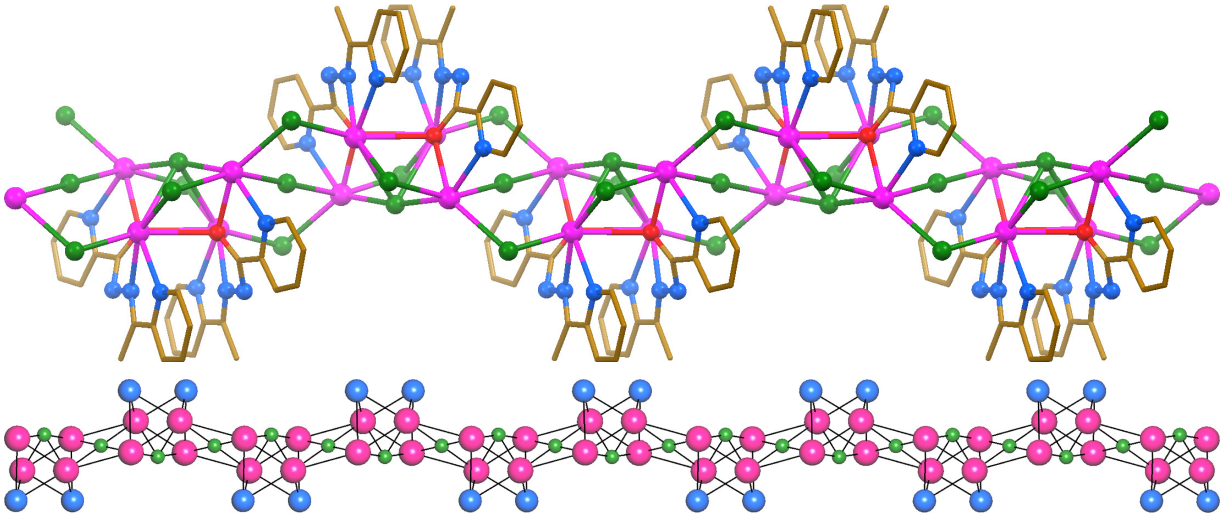

Figure 4. (top) Crystal structure of **[Pb$_2$(L^{IV})Cl$_3$]$_n$** (hydrogen atoms are omitted for clarity; color code: C = gold, N = blue, Cl = green, O = red, Pb = magenta). (bottom) A simplified underlying network of **[Pb$_2$(L^{IV})Cl$_3$]$_n$** with the unique pentanodal 3,4,4,5,6-connected chain topology ***sda*2** defined by the point symbol of $(3\cdot4^2)_2(3^2\cdot4^2\cdot5^2)(3^2\cdot4^3\cdot5)(3^3\cdot4^3\cdot5^3\cdot6)_2(3^3\cdot4^5\cdot5^5\cdot6^2)_2$ (color code: **L^{IV}** = blue, Cl = green, Pb = magenta).

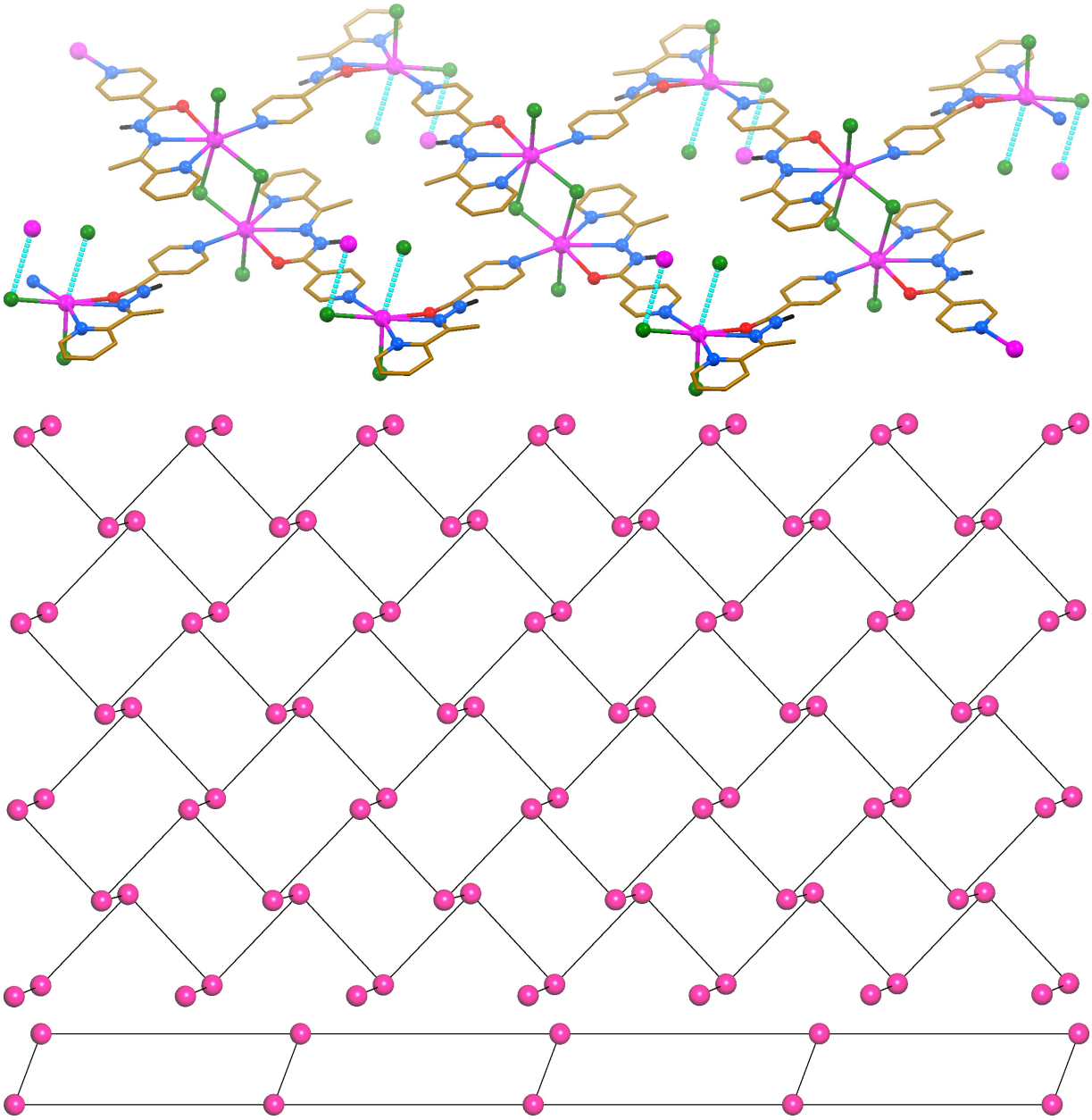

Figure 5. (top) Crystal structure of **[Pb(HL^{V})Cl$_2$]$_n$** (CH hydrogen atoms are omitted for clarity; color code: C = gold, N = blue, Cl = green, O = red, Pb = magenta). Tetrel bonds Pb···Cl are shown as dashed lines. (middle) A simplified underlying network of **[Pb(HL^{V})Cl$_2$]$_n$**, considering tetrel bonds, with the uninodal 3-connected plane topology **hcb** (Shubnikov hexagonal plane net) defined by the point symbol of (6^3). (bottom) A simplified underlying network of **[Pb(HL^{V})Cl$_2$]$_n$**, without tetrel bonds, with the **SP 1-periodic net** (4,4)(0,2) topology defined by the point symbol of ($4^2{\cdot}6$) (color code: Pb = magenta).

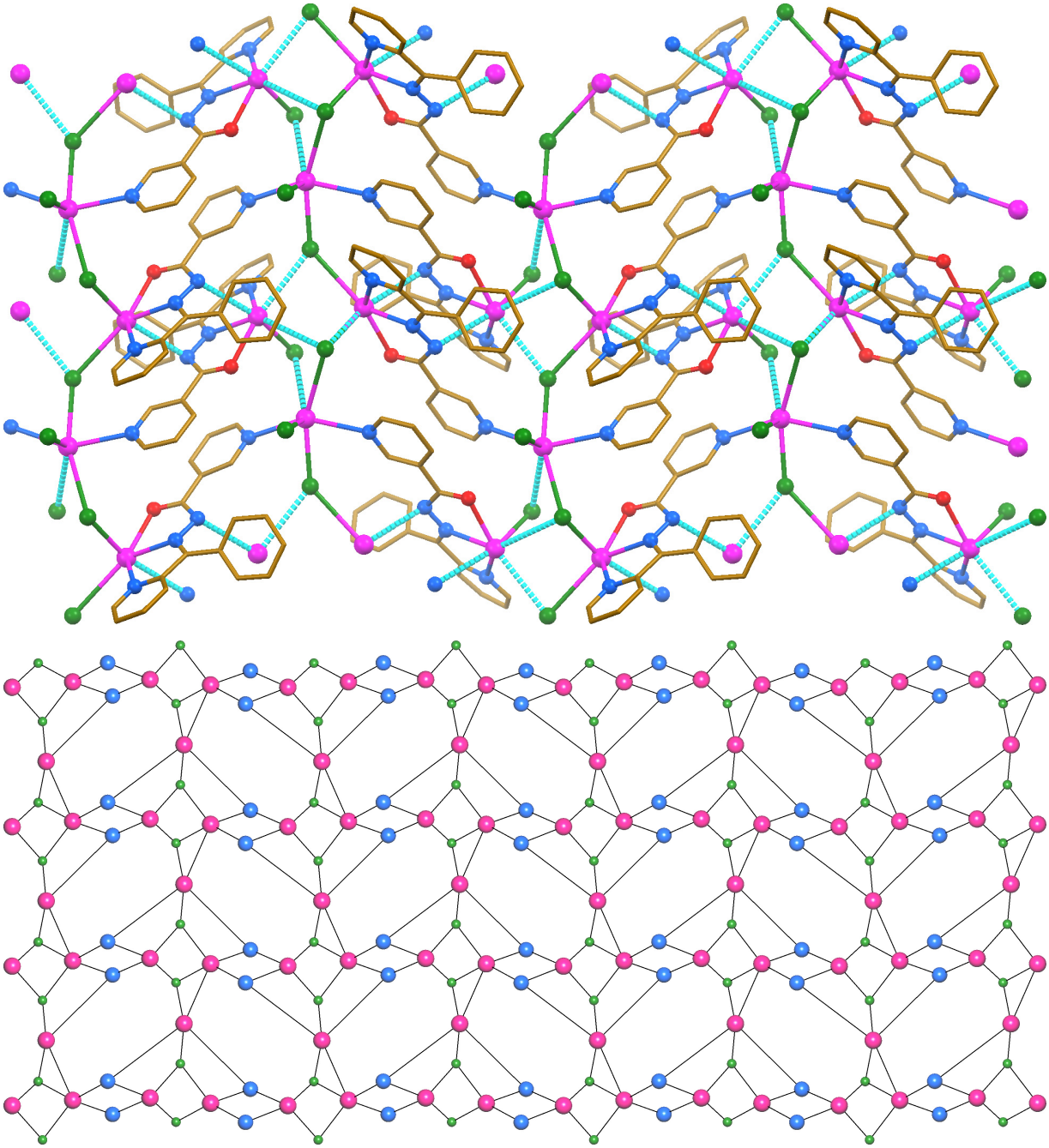

Figure 6. (top) Crystal structure of **[Pb$_3$(L^{VI})$_2$Cl$_4$]$_n$·nMeOH** (hydrogen atoms are omitted for clarity; color code: C = gold, N = blue, Cl = green, O = red, Pb = magenta). Tetrel bonds Pb···Cl and Pb···N are shown as dashed lines. (bottom) A simplified underlying network of **[Pb$_3$(L^{VI})$_2$Cl$_4$]$_n$·nMeOH**, considering all tetrel bonds, with the unique heptanodal 3,3,3,3,4,5,5-connected layer topology ***sda*3** defined by the point symbol of $(3{\cdot}4{\cdot}5)(3{\cdot}4^2{\cdot}6{\cdot}7^2{\cdot}8^2{\cdot}9^2)(3{\cdot}4^3{\cdot}5{\cdot}6^2{\cdot}7^2{\cdot}8)(4^2{\cdot}6)_2(4^3{\cdot}6^2{\cdot}7)(4^3)$ (color code: **L^{VI}** = blue, Cl = green, Pb =

magenta).

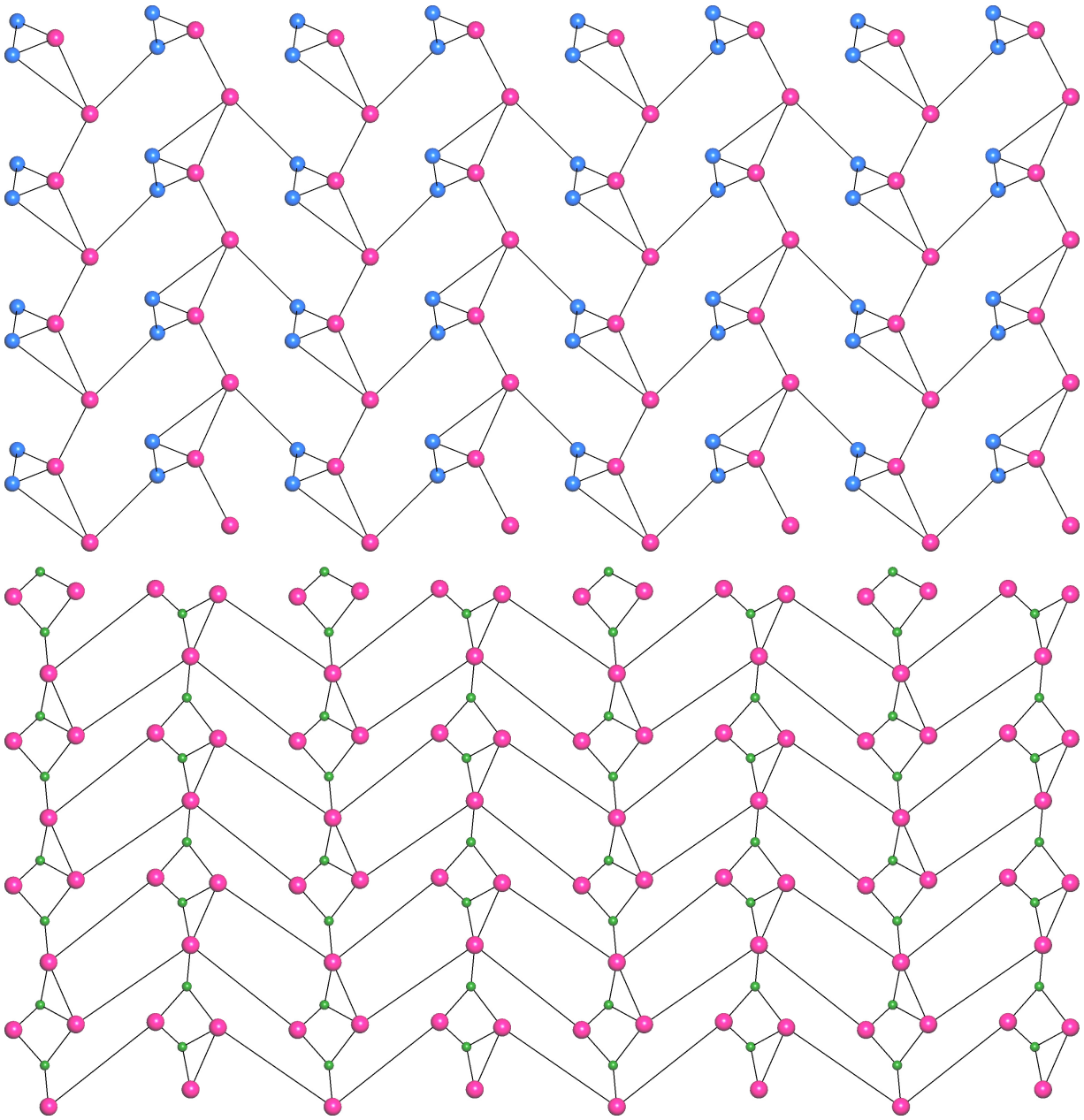

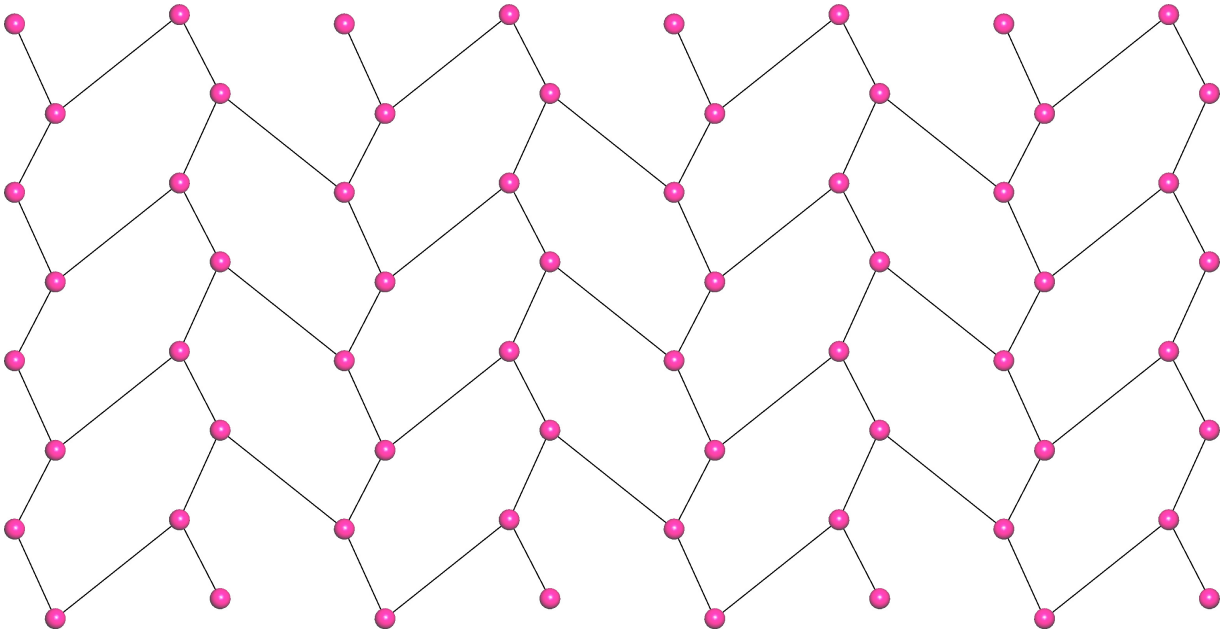

Figure 7. (top) A simplified underlying network of **[Pb$_3$(L^{VI})$_2$Cl$_4$]$_n$·nMeOH**, considering all the Pb···N tetrel bonds, with the unique tetranodal 3,3,4,4-connected layer topology **3,3,4,4L1** defined by the point symbol of $(3{\cdot}8^2)(3{\cdot}8^4{\cdot}9)(3^2{\cdot}4{\cdot}8^2{\cdot}9)(3^2{\cdot}4)$. (middle) A simplified underlying network of **[Pb$_3$(L^{VI})$_2$Cl$_4$]$_n$·nMeOH**, considering all the Pb···Cl tetrel bonds, with the unique pentanodal 3,3,3,4,5-connected layer topology **3,3,3,4,5L1** defined by the point symbol of $(3{\cdot}4{\cdot}5^2{\cdot}6^2)(3{\cdot}4{\cdot}5)(3{\cdot}5^2{\cdot}6^4{\cdot}8{\cdot}9^2)(4{\cdot}5{\cdot}6)(4{\cdot}6^2)$. (bottom) A simplified underlying network of **[Pb$_3$(L^{VI})$_2$Cl$_4$]$_n$·nMeOH**, without tetrel bonds, with the uninodal 3-connected plane topology **hcb** (Shubnikov hexagonal plane net) defined by the point symbol of (6^3) (color code: **L^{VI}** = blue, Cl = green, Pb = magenta).

Table 1. Covalent and Tetrel Bond Lengths (Å) in the Structures of Pb^{II} Complexes Described in this Work

Complex	Bond	Bond donor	Bond length	Bond type
$[Pb_2(L^{I})Cl_4]_n$	Pb–N	L	2.563(12)	covalent
	Pb–Cl	Cl^-	2.766(4)	covalent
		Cl^-	2.859(4)	covalent
		Cl^-	2.903(4)	covalent
		Cl^-	2.980(4)	covalent
		Cl^-	3.203(4)	covalent
		Cl^-	3.245(4)	covalent
$[Pb(HL^{II})Cl_2]_n$·nMeOH	Pb–N	L	2.545(10)	covalent
		L	2.780(11)	covalent
		L	3.391(11)	tetrel
	Pb–O	L	2.770(9)	covalent
		Cl^-	2.696(3)	covalent
		Cl^-	2.716(4)	covalent
		Cl^-	3.066(3)	covalent
$[Pb(HL^{III})Cl_2]_n$·0.5nMeOH	Pb–N	L	2.709(5)	covalent
		L	2.712(6)	covalent
		L	2.813(7)	covalent
	Pb–O	L	2.682(5)	covalent
	Pb–Cl	Cl^-	2.796(2)	covalent
		Cl^-	2.884(2)	covalent
		Cl^-	2.948(2)	covalent
$[Pb_2(L^{IV})Cl_3]_n$	Pb–N	L	2.468(3)	covalent
		L	2.513(3)	covalent
		L	2.534(3)	covalent
	Pb–O	L	2.415(2)	covalent
			2.832(3)	covalent
			2.839(3)	covalent

	Pb–Cl	Cl^-	2.7839(10)	covalent
		Cl^-	2.8262(11)	covalent
		Cl^-	2.8366(2)	covalent
		Cl^-	2.9231(2)	covalent
		Cl^-	3.0279(10)	covalent
		Cl^-	3.0445(9)	covalent
		Cl^-	3.2221(9)	covalent
$[Pb(HL^V)Cl_2]_n$	Pb–N	L	2.587(8)	covalent
		L	2.626(8)	covalent
		L	2.723(9)	covalent
		L	2.743(9)	covalent
		L	2.784(10)	covalent
		L	2.872(10)	covalent
	Pb–O		2.824(7)	covalent
			2.849(8)	covalent
	Pb–Cl	Cl^-	2.642(3)	covalent
		Cl^-	2.779(3)	covalent
		Cl^-	2.812(4)	covalent
		Cl^-	2.814(3)	covalent
		Cl^-	2.983(4)	covalent
		Cl^-	3.382(4)	tetrel
$[Pb_3(L^{VI})_2Cl_4]_n$·nMeOH	Pb–N	L	2.458(15)	covalent
		L	2.474(16)	covalent
		L	2.557(15)	covalent
		L	2.624(17)	covalent
		L	2.660(16)	covalent
		L	2.684(17)	covalent
		L	2.989(15)	tetrel
		L	3.093(15)	tetrel
	Pb–O	L	2.384(13)	covalent

	L	2.403(13)	covalent
Pb–Cl	Cl^-	2.593(6)	covalent
	Cl^-	2.645(6)	covalent
	Cl^-	2.723(6)	covalent
	Cl^-	2.763(5)	covalent
	Cl^-	3.195(5)	covalent
	Cl^-	3.196(5)	covalent
	Cl^-	3.440(5)	tetrel
	Cl^-	3.467(6)	tetrel
	Cl^-	3.490(6)	tetrel

Table 2. Classic Hydrogen Bond Lengths (Å) and Angles (°) for $[Pb(HL^{II})Cl_2]_n$·nMeOH, $[Pb(HL^{III})Cl_2]_n$·0.5nMeOH and $[Pb_3(L^{VI})_2Cl_4]_n$·nMeOH

Compound	D–H···A	*d*(D–H)	*d*(H···A)	*d*(D···A)	∠(DHA)
$[Pb(HL^{II})Cl_2]_n$·nMeOH	N(2)–H(2N)···O(2)	0.88	2.01	2.862(15)	163
$[Pb(HL^{III})Cl_2]_n$·0.5nMeOH[a]	N(3)–H(3N)···Cl(1)$^{\#1}$	0.91(7)	2.36(6)	3.219(7)	159(6)
	O(2)–H(2O)···Cl(1)$^{\#2}$	0.90(14)	2.71(15)	3.284(18)	123(10)
	O(2)–H(2O)···O(1)$^{\#2}$	0.90(14)	2.50(14)	3.166(19)	131(12)
$[Pb_3(L^{VI})_2Cl_4]_n$·nMeOH	O(41)–H(41)···Cl(4)$^{\#2}$	0.82	2.32	3.13(2)	169

[a]Symmetry transformations used to generate equivalent atoms: #1 1 + *x*, *y*, *z*; #2 –1 – *x*, 1 – *y*, 2 – *z*.

Table 3. π···π Distances (Å) and Angles (°) for $[Pb(HL^{II})Cl_2]_n$·nMeOH, $[Pb(HL^{III})Cl_2]_n$·0.5nMeOH, $[Pb(HL^{V})Cl_2]_n$ and $[Pb_3(L^{VI})_2Cl_4]_n$·nMeOH[a]

	Cg(*I*)	Cg(*J*)	*d*[Cg(*I*)–Cg(*J*)]	*α*	*β*	*γ*	slippage
$[Pb(HL^{II})Cl_2]_n$·nMeOH[b]	Cg(2)	Cg(3)$^{\#1}$	3.748(7)	5.4(6)	21.6	23.8	1.379
	Cg(3)	Cg(2)$^{\#1}$	3.748(7)	5.4(6)	23.8	21.6	1.510
	Cg(3)	Cg(3)$^{\#2}$	3.512(7)	0.0(6)	11.9	11.9	0.722
$[Pb(HL^{III})Cl_2]_n$·0.5nMeOH[c]	Cg(1)	Cg(2)$^{\#1}$	3.790(4)	6.8(4)	19.4	25.0	1.260
	Cg(2)	Cg(1)$^{\#2}$	3.791(4)	6.8(4)	25.0	19.4	1.600
	Cg(2)	Cg(2)$^{\#3}$	3.734(4)	0.0(3)	25.0	25.0	1.579
$[Pb(HL^{V})Cl_2]_n$[d]	Cg(3)	Cg(6)$^{\#1}$	3.559(6)	3.0(5)	20.5	20.3	1.245
	Cg(3)	Cg(6)$^{\#2}$	3.772(6)	2.3(5)	23.8	22.6	1.523
	Cg(4)	Cg(5)$^{\#1}$	3.586(6)	3.2(5)	20.7	19.3	1.265
	Cg(4)	Cg(5)$^{\#3}$	3.625(6)	4.2(5)	14.1	17.5	0.885
	Cg(5)	Cg(4)$^{\#4}$	3.586(6)	3.2(5)	19.3	20.7	1.187
	Cg(5)	Cg(4)$^{\#3}$	3.625(6)	4.2(5)	17.5	14.1	1.090
	Cg(6)	Cg(3)$^{\#4}$	3.559(6)	3.0(5)	20.3	20.5	1.236
	Cg(6)	Cg(3)$^{\#2}$	3.772(6)	2.3(5)	22.6	23.8	1.449
$[Pb_3(L^{VI})_2Cl_4]_n$·nMeOH[e]	Cg(5)	Cg(7)$^{\#1}$	3.727(12)	7	26.2	27.7	1.643
	Cg(5)	Cg(8)$^{\#2}$	3.748(11)	16	16.7	28.2	1.077
	Cg(5)	Cg(10)$^{\#3}$	3.727(12)	7	26.1	27.7	1.642
	Cg(6)	Cg(7)$^{\#4}$	3.644(11)	14	23.7	11.0	1.466
	Cg(6)	Cg(10)$^{\#5}$	3.644(11)	14	23.7	11.0	1.467
	Cg(7)	Cg(5)$^{\#6}$	3.728(12)	7	27.7	26.2	1.732
	Cg(7)	Cg(6)$^{\#2}$	3.643(11)	14	11.0	23.7	0.694
	Cg(8)	Cg(5)$^{\#4}$	3.749(11)	16	28.2	16.7	1.772
	Cg(10)	Cg(5)$^{\#3}$	3.728(12)	7	27.7	26.1	1.731
	Cg(10)	Cg(6)$^{\#7}$	3.643(11)	14	11.0	23.7	0.694

[a]Cg(*I*)–Cg(*J*): distance between ring centroids; *α*: dihedral angle between planes Cg(*I*) and Cg(*J*); *β*: angle Cg(*I*) → Cg(*J*) vector and normal to plane *I*; *γ*: angle Cg(*I*) → Cg(*J*) vector and normal to plane *J*; slippage: distance between Cg(*I*) and perpendicular projection of Cg(*J*) on ring *I*.

[b]Symmetry transformations used to generate equivalent atoms: #1 –*x*, 1 – *y*, –*z*; #2 –*x*, 2 – *y*, –*z*. Cg(2): N(1)–C(13)–C(12)–C(11)–C(10)–C(14), Cg(3): N(4)–C(23)–C(22)–C(21)–C(20)–C(24).

[c]Symmetry transformations used to generate equivalent atoms: #1 *x*, 1 + *y*, *z*; #2 *x*, –1 + *y*, *z*; #3 –1 – *x*, –*y*, 1 – *z*.

Cg(1): N(1)–C(1)–C(2)–C(3)–C(4)–C(5), Cg(2): N(4)–C(9)–C(8)–C(12)–C(11)–C(10).
[d]Symmetry transformations used to generate equivalent atoms: #1 –*x*, 1/2 + *y*, 1/2 – *z*; #2 –*x*, 2 – *y*, 1 – *z*; #3 –*x*, 1 – *y*, 1 – *z*; #4 –*x*, –1/2 + *y*, 1/2 – *z*. Cg(3): N(1)–C(1)–C(2)–C(3)–C(4)–C(5), Cg(4): N(4)–C(11)–C(10)–C(9)–C(13)–C(12), Cg(5): N(5)–C(14)–C(15)–C(16)–C(17)–C(18), Cg(6): N(8)–C(24)–C(23)–C(22)–C(26)–C(25).
[e]Symmetry transformations used to generate equivalent atoms: #1 *x*, 1/2 – *y*, –1/2 + *z*; #2 *x*, –1 + *y*, *z*; #3 *x*, *y*, *z*; #4 *x*, 1 + *y*, *z*; #5 *x*, 3/2 – *y*, 1/2 + *z*; #6 *x*, 1/2 – *y*, 1/2 + *z*; #7 *x*, 3/2 – *y*, –1/2 – *z*. Cg(5): N(1)–C(1)–C(2)–C(3)–C(4)–C(5), Cg(6): N(4)–C(8)–C(9)–C(10)–C(11)–C(12), Cg(7): N(11)–C(25)–C(24)d–C(23)d–C(22)d–C(21)d, Cg(8): N(14)–C(28)–C(29)–C(30)–C(31)–C(32), Cg(10): C(21)–C(22)–C(23)–C(24)–C(25)c–N(11)c.